NSRRC-J01483 (2014)

Macromolecules

Article

pubs.acs.org/Macromolecules

Directing the Interfacial Morphology of Hierarchical Structures of Dendron-Jacketed Block Copolymers via Liquid Crystalline Phases

Wei-Tsung Chuang,*[,†] Ting-Ya Lo,[‡] Yen-Chih Huang,[†] Chun-Jen Su,[†] U-Ser Jeng,*[,†,‡] Hwo-Shuenn Sheu,[†] and Rong-Ming Ho[‡]

[†]National Synchrotron Radiation Research Center, Hsinchu 30076, Taiwan

[‡]Department of Chemical Engineering, National Tsing Hua University, Hsinchu 30013, Taiwan

Supporting Information

ABSTRACT: Interfacial morphologies of hierarchically phase-separated domains in supramolecular dendron-jacketed block copolymers (DJBCP) are directed via liquid-crystalline (LC) phases of the dendronized blocks. The DJBCP is formed with a dendron 4′-(3,4,5-trioctyloxybenzoyloxy)benzoic acid (TOB), selectively incorporated into the P4VP block of poly(styrene)-*block*-poly(4-vinylpyridine) (PS-*b*-P4VP). Revealed from small- and wide-angle X-ray scattering as well as transmission electron microscopy, the hexagonally packed columnar LC phase (HEX_{col}) of the dendronized blocks P4VP(TOB) can substantially decrease the curvature of the intermaterial dividing surfaces (IMDS) of the DJBCP. Consequently formed are hierarchically structured DJBCP with hexagonally packed hexagon PS cylinders. As the locally two-dimensionally (2D)-ordered HEX_{col} phase reduces to 1D ordered smectic (Sm) phase with weakened LC packing strength, the planar IMDS of the DJBCP relaxes into curved IMDS for circular PS cylinders. IMDS flattening effect imposed by the columnar LC phase is further strengthened via a triblock DJBCP of P4VP(TOB)$_x$-*b*-PS-*b*-P4VP(TOB)$_x$, leading to a highly oriented honeycomb structure with an ordering length up to sub-millimeter. The LC-controlled IMDS morphology of the DJBCP might facilitate fabrication of templates toward nanoperiodic arrays with sharp channel edges for lithography applications.

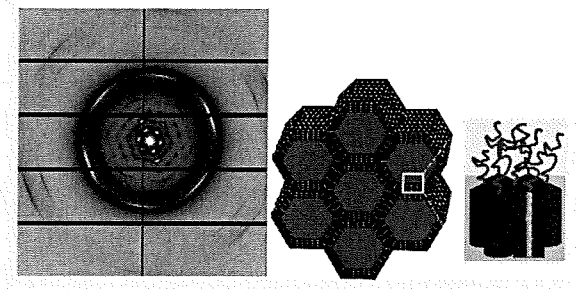

INTRODUCTION

Recent progress in nanoscience and nanotechnology has advanced greatly the morphological controls on block copolymer (BCP) based nanostructures. In particular, the precision has reached a nanometer scale, leading to promising BCP templates with nanoperiodic arrays for lithographic applications of next-generation microelectronics.[1] Controlling the interfacial morphology of self-assembled BCP microdomains remains, however, a formidable task. For example, circular cylinders are commonly observed in cylinder-forming block copolymers because intermaterial-dividing surfaces (IMDS) favor, in general, minimized interfaces with constant mean curvatures.[2] Atypical IMDS features of BCP microdomains, such as hexagonal,[3−5] diamond,[6] and rectangular[7,8] cylinders, nevertheless, could be formed in complicated block copolymer systems of multiblock, star, and rod−coil copolymers. For instance, polyhedral cylinders were observed via partial removal of small pendant molecules in block copolymer-based supramolecules.[9] Deformation for polyhedral colloidal particles owing to packing frustration of the block copolymer tail was also reported.[10,11] These works demonstrated that the copolymer junction per molecule, conformational asymmetry among blocks, molecular architecture, packing frustration, and processing routes could all be utilized in tailoring IMDS features. Fine controls of the IMDS are of interest in fabrications of novel nanostructured templates for advanced lithographic applications.

Morphology control with side-chain-functionalized supramolecules at a nanometer scale has enabled many exciting materials with tailored functions. The pioneer group of Ikkala[12−14] showed that pentadecylphenol (PDP) surfactants could passively form a smectic liquid crystal (LC) phase in the microdomains of poly(styrene)-*block*-poly(4-vinylpyridine) (PS-*b*-P4VP), with the microphase separation dominated by the two repulsive dissimilar copolymer blocks. Shearing aligned supramolecular structures based on PS-*b*-P4VP(PDP) were further investigated by Brinke and Ikkala et al.[15,16] With reinforced LC packing strength, several hierarchical structures based on columnar LC phases were found in dendronized polymers,[17−19] dendrimers,[20] and dendronized block copolymer systems.[21−23] Moreover, Mezzenga and co-workers[17−20] reported that dendronized polymers or dendrimers incorporated with anionic lipids could form rich columnar LC phases with various lattice parameters. They also reported that cationic dendronized block copolymers could self-organize into novel hierarchical structures including rectangularly, tetragonally, and hexagonally packed columns within lamellar microdomains.[21]

Received: May 27, 2014
Revised: July 31, 2014
Published: August 19, 2014

 © 2014 American Chemical Society

Scheme 1. Schematic Illustration of a Supramolecular Complex of PS_m-*b*-$P4VP_n(TOB)_x$

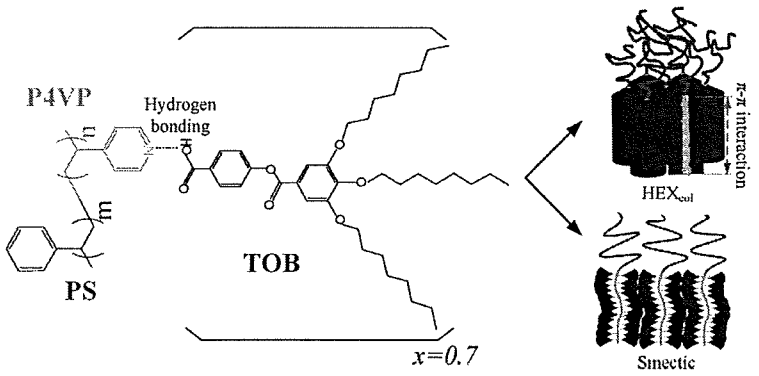

Recently, we reported a novel supramolecular dendron-jacketed block copolymer (DJBCP), with the dendron 4′-(3,4,5-trioctyloxybenzoyloxy)benzoic acid (TOB) selectively incorporated into the P4VP blocks of PS-*b*-P4VP via hydrogen bonding (Scheme 1) for PS-*b*-P4VP(TOB)$_x$.[22,23] Various hierarchical morphologies of the DJBCP, such as lamellae, hexagonally packed cylinders, face-center-cubic spheres, and tetragonally perforated layers, were obtained via modulating the TOB grafting density between x = 0.2–0.7. With the highest grafting ratio x = 0.7, the dendronized blocks P4VP(TOB)$_{0.7}$ could form either hexagonally packed columns (HEX$_{col}$) or smectic (Sm) LC phases, depending on a selected processing route;[23] correspondingly, the global structure of the supramolecular complex PS-*b*-P4VP(TOB)$_{0.7}$ evolved from a face-center-cubic structure to tetragonally perforated layers, as the local LC packing strengthened from Sm to HEX$_{col}$.[23] Interplay between the microphase separation of the supramolecular block copolymer and the LC ordering of P4VP(TOB)$_x$ was elucidated previously with temperature-dependent small- and wide-angle X-ray scattering (SAXS/WAXS) for the formation mechanism of the hierarchically ordered structures observed.[22,23] Nevertheless, how the local LC packing could affect the interfacial morphology of a hierarchically ordered DJBCP was not addressed fully in our previous studies.[22,23] Considering that the columnar LC phase P4VP(TOB)$_{0.7}$ could already direct the microphase separation of the PS-*b*-P4VP host for tetragonally perforated layers of flat IMDS as mentioned above,[22] we believe that it is possible to flatten the IMDS morphology of similar DJBCP hierarchical structures via reinforced LC ordering strength. Such IMDS control with LC phases of DJBCP may lead to lithographic templates of nanoperiodic arrays with sharp channel edges.

In this study, we demonstrate modulations of the IMDS morphology of hierarchically ordered DJBCP via local LC packing for the first time. AB DJBCP of PS_m-*b*-$P4VP_n(TOB)_x$ of different m/n ratios are synthesized for different hierarchical morphologies, with a fixed x value of 0.7 for optimized LC packing strength. We further successfully enhance the IMDS control with an ABA DJBCP analogy, having an increased interface area per PS block for larger LC influences. Consequently, novel and column-based hierarchical structures with flat IMDS, such as honeycomb morphology and highly asymmetric lamellae, can be obtained, as revealed from SAXS/WAXS and transmission electron microscopy (TEM). We demonstrate that the designated columnar LC phase not only flattens the IMDS but also directs the long-range ordering of the DJBCP for hierarchical order–order transitions.

EXPERIMENTAL SECTION

DJBCP of PS_m-*b*-$P4VP_n(TOB)_x$ were prepared with different m/n ratios. The TOB grafting density x was kept at 0.7 to form rigid LC columns of P4VP(TOB)$_{0.7}$. The molecular features of PS_m-*b*-$P4VP_n(TOB)_{0.7}$ are listed in Table 1, including the ideal-mixing volume fractions of the dendronized blocks P4VP(TOB)$_{0.7}$ ($\phi_{0\text{-DB}}$), calculated based on the densities of PS (1.047 g cm^{-3}), P4VP (1.114 g cm^{-3}), and TOB (1.112 g cm^{-3}), without LC packing.[22] All PS_m-*b*-$P4VP_n$ from Polymer Source Inc. were used without further purification. TOB dendron, 4′-(3,4,5-trioctyloxybenzoyloxy)benzoic acid, was prepared according to our previous report.[11] Blend films of PS_m-*b*-$P4VP_n(TOB)_{0.7}$ were cast from chloroform solutions containing mixtures (1% by mass) of the copolymer and TOB. The as-cast thin films (thickness ca. 0.4 mm) were slowly dried under a controlled solvent vapor pressure at room temperatures for formation of a columnar LC phase. For highly oriented hierarchical structures, the as-cast thin films were stretched (Linkam TST 350) at 120 °C for a drawing ratio ca. 2, followed by isothermal annealing at 85 °C to release residual stress. For a trapped smectic phase, a similarly processed sample was quenched from 120 °C by using cold air jet for a cooling rate about 90 °C/min. These processed films were measured with SAXS and WAXS or used for sample preparation of transmission electron microscope (TEM).

Table 1. Molecular Features of the DJBCP Studied, Including $\phi_{0\text{-DB}}$ for the Volume Fraction of the Dendronized Block P4VP(TOB)$_{0.7}$ without LC Packing

sample	PS (g mol^{-1})	P4VP (g mol^{-1})	M_w/M_n	$\phi_{0\text{-DB}}$
PS_{230}-*b*-$P4VP_{90}(TOB)_{0.7}$	24 000	9500	1.1	0.67
PS_{288}-*b*-$P4VP_{22}(TOB)_{0.7}$	30 000	2400	1.1	0.29
$P4VP_{43}(TOB)_{0.7}$-*b*-PS_{260}-*b*-$P4VP_{43}(TOB)_{0.7}$	27 000	4500	1.09	0.62

Measurements of SAXS and WAXS were performed respectively at BL23A SWAXS and BL01C2 XRD Endstations of the National Synchrotron Radiation Research Center (NSRRC), Taiwan. SAXS data were collected with 15 keV X-rays of a wavelength 0.8265 Å, whereas WAXS data with 10 keV (1.2398 Å). All SAXS data collected with an area detector (MarCCD165 or Pilatus 1M-F) were rigorously corrected for electronic noise, sample transmission, background scattering, and detector sensitivity. The scattering intensity was calibrated with a sample of high-density polyethylene for absolute scattering intensity, whereas the scattering wavevector q defined by $4\pi\lambda^{-1}$ sin θ with scattering angle 2θ was calibrated with silver behenate, as detailed in a previous report.[24] One-dimensional (1D) SAXS profiles were circularly averaged from the corresponding 2D

dx.doi.org/10.1021/ma501105p | Macromolecules 2014, 47, 6047–6054

scattering patterns. WAXS data collected with an image plate (Mar345) were placed on the q-axis, calibrated with diffractions from mixed powders of silicon and silver behenate. For oriented structures, SAXS and WAXS patterns were recorded with three orthogonal beam incidences along the directions X, Y, and Z defined in Figure 1c, with Z being the stretching direction. Images of the DJBCP taken with the beam incidences respectively along the X and Z directions (Figure 1c) of a stretching-annealed film of AB DJBCP PS_{230}-b-$P4VP_{90}(TOB)_{0.7}$. The stretching-annealing process enabled highly oriented and ordered domains, allowing elucidation of relative orientations of the local LC phase and the global ordered phase of the DJBCP. Specifically, in the small-q region of Figure 1a, single-crystal-like sharp reflections observed can be well indexed with oblique 2D lattice parameters a = 32 nm, b = 35 nm, and β = 55° (i.e., a deformed hexagonal lattice). Furthermore, the reflections aligned along the Z-direction in the small-q region of Figure S1 reveal a highly oriented layering structure. Together, these two SAXS patterns suggest 2D obliquely packed cylinders (OBL_{CYL}), with the cylinder axis oriented perpendicular to the film-stretching direction (Z).

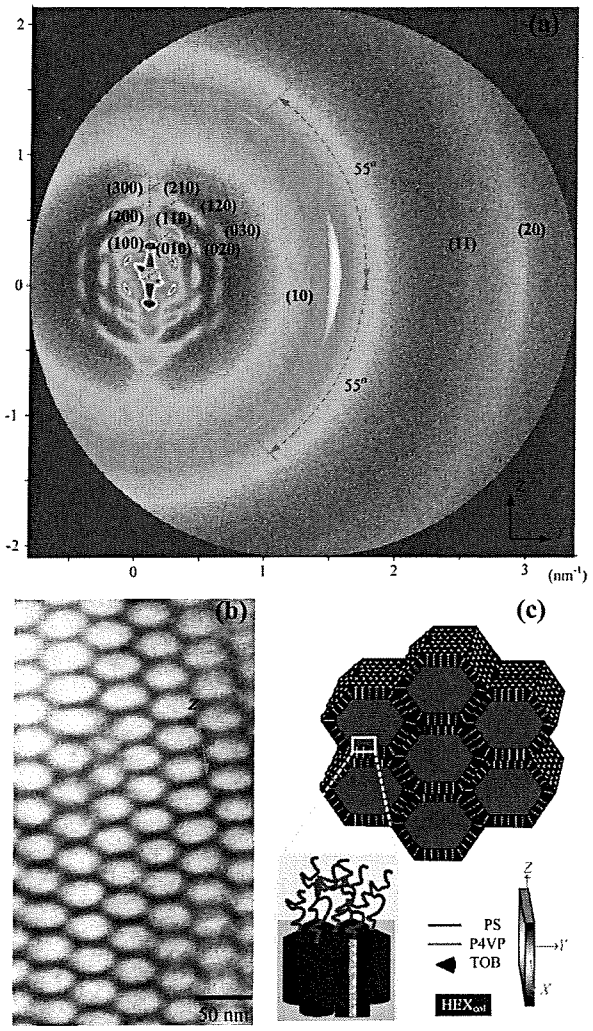

Figure 1. (a) SAXS pattern with the beam incidence along the PS cylindrical axis of a stretching-annealed sample of PS_{230}-b-$P4VP_{90}(TOB)_{0.7}$. (b) Corresponding TEM image for the OBL_{CYL} structure showing a honeycomb structure with hexagonal PS cylinders (bright domains). The arrow marks the sample stretching direction (Z). (c) Cartoons for the hierarchically structure HEX_{col}-*within*-OBL_{CYL} with hexagonal PS cylinders.

in real space were observed with a transmission electron microscope (JEOL, JEM-2100, accelerating voltage 200 kV). TEM samples were cryo-sectioned at −60 °C with an ultramicrotome (Leica Reichert Ultracut-E); sections of a thickness 90 nm were collected on a gold grid and stained with iodine vapor for ca. 30 min. TEM images were taken with varied sample orientations.

RESULTS AND DISCUSSION

DJBCP with the Majority of Dendronized Blocks. Shown in Figure 1a and Figure S1 are the 2D SAXS patterns

In the large-q region in Figure 1a, the arc-like reflections with peak position ratios of $1:\sqrt{3}:2$ can be identified as (10), (11), and (20) reflections of an HEX_{col} LC phase. A WAXS pattern covering the complete six sets of the HEX_{col} reflections is shown in Figure S2. These results indicate that the dendronized blocks could form highly oriented HEX_{col} LC domains (with a lattice parameter a_c = 4.9 nm extracted from the first peak position) within OBL_{CYL} for a hierarchically ordered HEX_{col}-*within*-OBL_{CYL} structure. Close scrutiny reveals that the included angle between the two sets of the HEX_{col} reflections marked in Figures 1a (also in Figure S3) is 55°, which corresponds well to the β angle of the global OBL lattice. The six sets of reflections of HEX_{col} are well aligned along the corresponding azimuthal directions, implying that the LC columns are oriented perpendicularly to the axial direction of the hexagonal PS cylinders, i.e. to the planar walls of the hexagonal Wigner–Seitz cells of the OBL lattice. Namely, fairly planar LC column domains (i.e., flat IMDS) are deployed along the edge planes of the hexagonal PS cylinders (as illustrated in Figure 1c). These highly oriented and sharp reflections (with small spreads in arc angles) of HEX_{col} strongly suggest hexagonal-like cylinders with flat IMDS morphology.

Furthermore, a TEM micrograph (Figure 1b) provides consistent evidence for the hierarchically ordered HEX_{col}-*within*-OBL_{CYL} with hexagonal PS cylinders. The cross sections of the hexagonal PS cylinders were found to be slightly compressed along the direction of stretching (Z) (as marked in Figure 1b). This might be caused by strain-induced alignment and lattice distortion during the uniaxial stretching annealing,[22] resulting in a preferred orientation of the LC columns along the stretching direction and, hence, compressed hexagons with larger planes oriented along the stretching direction. Correspondingly observed is the higher intensity for the set of (10), (11), and (20) reflections aligned along the Y-direction, in comparison with other reflection sets deviated from the Y-axis (as shown in Figure 1a and Figure S3). Figure 1c illustrates a schematic representation of the observed HEX_{col}-*within*-OBL_{CYL} structure of the PS_{230}-b-$P4VP_{90}(TOB)_{0.7}$ film. Because of packing frustration at corner zones of the Winger–Seitz cells of the OBL_{CYL} phase, the dendronized blocks of the local HEX_{col} LC phase would extend more to improve the space filling imposed by the Winger–Seitz cells.

To illustrate further the influence of LC ordering strength on the IMDS, we conducted SAXS for a stretched film of PS_{230}-b-$P4VP_{90}(TOB)_{0.7}$ during heating and quenching, for in-situ LC phase transitions. Figure 2 exhibits temperature-dependent SAXS profiles circularly averaged from the corresponding 2D SAXS patterns (Figure S4), showing a column-to-smectic LC

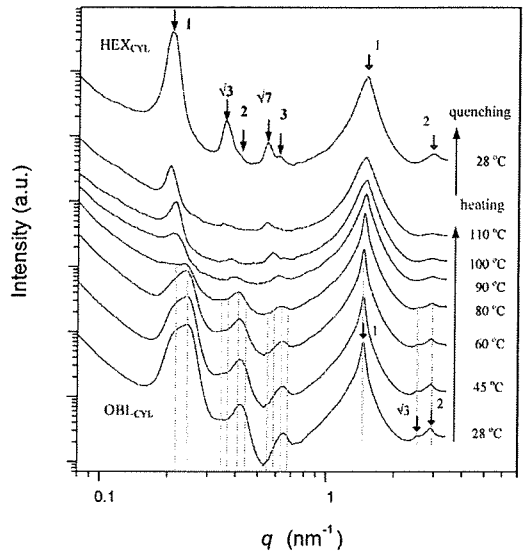

Figure 2. Temperature-dependent SAXS profiles for a hierarchical phase transition from HEX$_{col}$-*within*-OBL$_{CYL}$ to Sm-*within*-HEX$_{CYL}$. The expected reflections of the OBL lattice and LC columnar phase are indicated with the dotted lines, whereas those for HEX$_{CYL}$ and smectic phases are marked with the peak position ratios.

transition temperature $T_c \approx 90$ °C. The global OBL$_{CYL}$ structure persisted with a reasonable thermal stability below T_c. Above T_c, broad smectic rings could be observed in the large-q region together with the hexagonally packed cylinders (HEX$_{CYL}$) in the small-q region.

When the smectic phase was kinetically trapped by a rapid quenching from 110 to 28 °C, the SAXS pattern (Figure 3a) showed 6-fold symmetric reflections in the small-q region and could be characterized with HEX$_{CYL}$ of a lattice parameter a = 31.4 nm. Together with the broad smectic rings that correspond to a layer spacing 4.2 nm in the large-q region, the 2D SAXS pattern reveals a long-range ordered smectic-*within*-HEX$_{CYL}$ structure. We note that the HEX$_{col}$ LC phase of the P4VP(TOB)$_{0.7}$ should be a thermally stable phase, as the kinetically trapped smectic phase could return to the HEX$_{col}$ phase after a long-term annealing between 60 and 80 °C.[23] Such a LC phase transition is consistent with the conclusion of a previous report by Wang et al.[25] After the recovery of HEX$_{col}$ LC phase, the system transited to the HEX$_{col}$-*within*-HEX$_{CYL}$ structure (instead of OBL$_{CYL}$), as shown in Figure S5, due to the release of residual stress in the annealing.

Most importantly revealed in the large-q region in Figure 3a are powder rings from randomly oriented smectic domains of the dendronized blocks, in contrast to the previous 6-fold arc-like reflections of oriented HEX$_{col}$ LC domains (Figure 1a). The isotropically oriented smectic domains imply circular PS cylinders in the Sm-*within*-HEX$_{CYL}$ structure (Figure 3c), as confirmed by the TEM micrograph in Figure 3b. Moreover, the circular PS domains with ca. 21 nm diameter (as estimated from Figure 3b) are substantially smaller than the distorted hexagonal PS domains, of a long diagonal length ca. 34 nm (Figure 1b). Nevertheless, the global structure remains largely the same, with similar lattice parameters (hence, similar peak positions of the reflections) during the columnar-to-smectic LC phase transition. These results demonstrate a fine control of IMDS morphology of DJBCP enabled by LC packing strength.

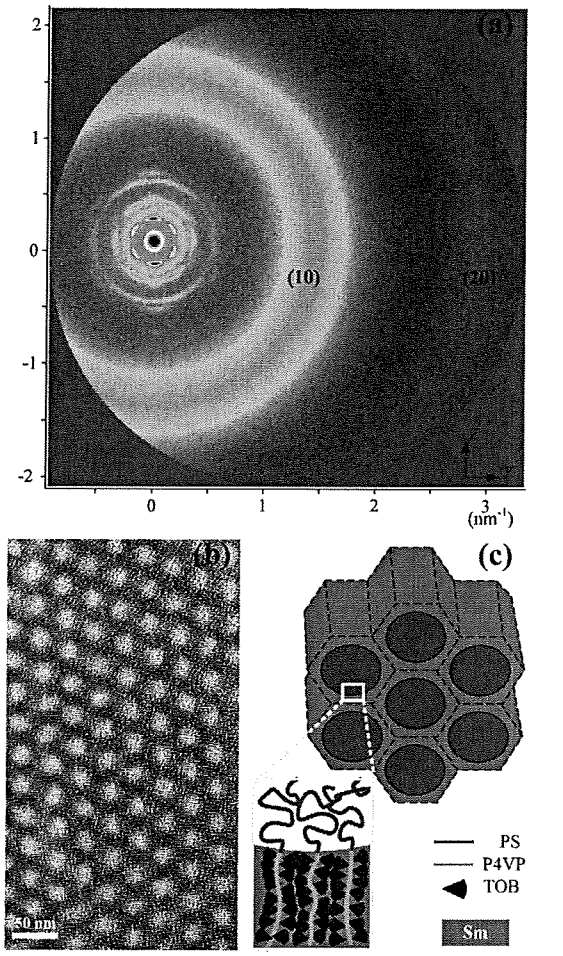

Figure 3. (a) SAXS pattern with the beam incidence along the PS cylindrical axis of the PS$_{230}$-*b*-P4VP$_{90}$(TOB)$_{0.7}$ film after a rapid quenching process. (b) Corresponding TEM image showing a HEX$_{CYL}$ structure with circular PS cylinders (bright domains). (c) Cartoons for the hierarchically structure of HEX$_{col}$-*within*-HEX$_{CYL}$ with circular PS cylinders.

We emphasize that the volume fraction ϕ_{DB} of P4VP-(TOB)$_{0.7}$ is dynamic in the system discussed, depending on the LC packing strength. When the LC packing strength is weakened (with the smectic phase), ϕ_{DB} = 0.70 estimated from the SAXS and TEM results (Figures 2 and 3b) is close to the value for ideal mixing $\phi_{0\text{-}DB}$ = 0.67, and the majority of dendron-jacked domains behave as the matrix phase. With a strong columnar LC packing (HEX$_{col}$), the P4VP(TOB)$_{0.7}$ block reverses to a minor phase with ϕ_{DB} = 0.41 (as estimated from the SAXS and TEM results in Figure 1), but this minor phase could remain as a continuous matrix phase to form "phase-inverted cylinders" owing to a high curvature energy that favors flattened IMDS (Figure 1b) with restrained chain conformations of PS and P4VP blocks (either extension or compression as discussed below). Similarly, previous studies on dendronized polymer–lipid supramolecular complexes[17] showed that a major phase of lipids with a fully stretched conformation could form cylinder domains. These results indicate that both the interfacial and conformational energies

dx.doi.org/10.1021/ma501105p | *Macromolecules* 2014, 47, 6047–6054

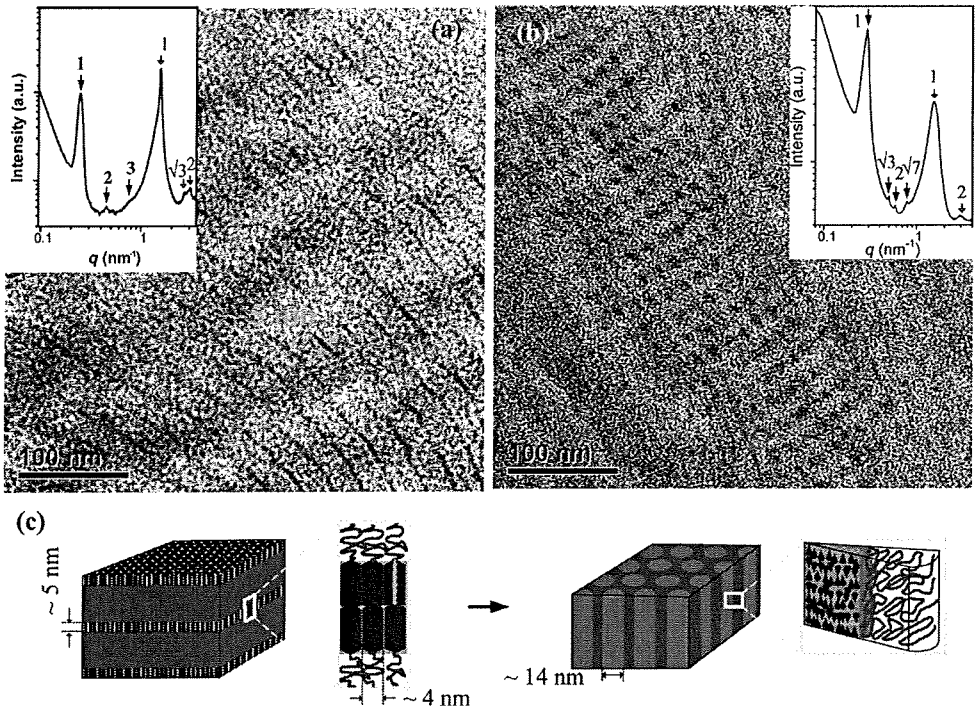

Figure 4. (a) SAXS profile and TEM micrograph for an as-cast film of PS_{288}-*b*-$P4VP_{22}(TOB)_{0.7}$ and (b) that for the film quenched from 120 °C. (c) Cartoons for the HEX_{col}-*within*-LAM structure (right) and Sm-within-HEX_{CYL} (left).

play an important role in minimizing the free energy of the system for unusual IMDS morphologies of the DJBCP.

DJBCP with a Minority of Dendronized Blocks. The HEX_{col} LC phase formed with a minority of dendronized blocks, of a volume fraction $\phi_{0\text{-DB}} = 0.29$, was found to override the microphase-separation behavior of PS_{288}-*b*-$P4VP_{22}(TOB)_{0.7}$. In the inset of Figure 4a, the SAXS profile shows ordered lamellar (LAM) reflections in the small-q region and three sharp reflections of peak position ratios $1:\sqrt{3}:2$ in the large-q region, indicating a hierarchical HEX_{col}-*within*-LAM structure. The extracted lamellar spacing is 25.4 nm; the lattice parameter a_c of the HEX_{col} LC phase is 4.7 nm. The corresponding TEM micrograph (Figure 4a) exhibits a highly asymmetric lamellar structure, with asymmetric sublayer thicknesses ca. 20 nm for the PS domains and 5 nm for the domains of the dendronized block. The highly asymmetric lamellae elucidate dramatic effects of the 2D-ordered HEX_{col} LC phase on flattening IMDS for layering domains rather than common observed cylinder domains, with the minor phase $\phi_{0\text{-DB}} = 0.29$ in DJBCP.

After thermal annealing for a columnar-to-smectic LC phase transition, this column-stabilized asymmetric LAM structure, kinetically trapped in a quenching process, transformed back to thermodynamically favored circular $P4VP(TOB)_{0.7}$ cylinders with a hexagonal packing, together with a smectic LC phase. SAXS and TEM shown in Figure 4b provide consistent evidence for a hierarchical structure of Sm-*within*-HEX_{CYL}. Molecular arrangements for the hierarchical order–order phase transformation are illustrated in Figure 4c, revealing the transformation from the HEX_{col}-*within*-LAM structure with flat IMDS to the Sm-*within*-HEX_{CYL} structure with IMDS of constant mean curvatures. Herein, the extremely asymmetric lamellar morphology manifests especially the high strength of the HEX_{col} LC phase on flattening the IMDS morphology. In contrast to the formation of cylinder domains by a columnar LC phase reported previously with peptide[26] or rod–coil based[27,28] block copolymers, the HEX_{col} LC phase of PS_{288}-*b*-$P4VP_{22}(TOB)_{0.7}$ could not be formed in the minor phase with cylinder domains. This may be attributed to that very limited cylindrical domains of dendronized blocks of 14 nm in diameter would not be able to accommodate many LC columns of 4 nm in diameter for a reasonable size of 2D-rodered HEX_{col} LC domains. In addition, the tunable LC phases (columnar or smectic phase) of the DJBCP provide more flexibility on tuning hierarchical self-assemblies.

ABA Triblock Architecture of DJBCP. To further enhance the flattening effect of the HEX_{col} LC phase on the IMDS of DJBCP, we have further designed an ABA DJBCP. The triblock $P4VP_{43}(TOB)_{0.7}$-*b*-PS_{260}-*b*-$P4VP_{43}(TOB)_{0.7}$ has a similar volume fraction of the dendronized block ($\phi_{0\text{-DB}} = 0.62$) but with approximately a half chain length, compared to that for the dendronized block of PS_{230}-*b*-$P4VP_{90}(TOB)_{0.7}$. With two block junctions per molecule in the ABA triblock architecture, the DJBCP could have even greater IMDS influences from the columnar LC phase, resulting in more rigid or better flattened IMDS for either asymmetric lamellae or hexagonal PS cylinders in HEX_{CYL} (*vide infra*). The SAXS pattern in Figure 5a, recorded from an as-cast sample of the ABA DJBCP, reveals features of a hierarchical HEX_{col}-*within*-LAM structure; these include lamellar reflections with peak position ratios 1:2:3:4 in the small-q region and three arc-like reflections positioned with the ratios $1:\sqrt{3}:2$ in the high-q region for an HEX_{col} LC phase. The corresponding lamellar spacing is 23.3 nm for the global LAM structure, whereas the lattice parameter a_c is 4.7 nm for the local HEX_{col} LC phase. The corresponding TEM micrograph in Figure 5b shows a layer thickness ca. 7.5 nm

dx.doi.org/10.1021/ma501105p | *Macromolecules* 2014, 47, 6047–6054

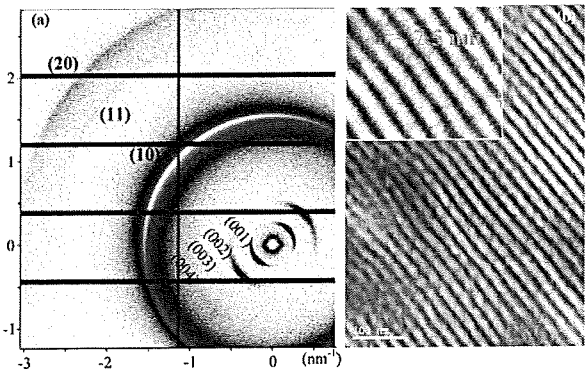

Figure 5. (a) SAXS pattern taken with a beam incidence along the film normal direction (Y) for an as-cast film of ABA BJBCP, $P4VP_{43}(TOB)_{0.7}$-*b*-PS_{260}-*b*-$P4VP_{43}(TOB)_{0.7}$. (b) Corresponding TEM micrograph showing the orientation of the local HEX_{col} (inset) within the global LAM structure.

for the HEX_{col} LC domains, having flat IMDS with PS layers (bright domains). Such HEX_{col}-*within*-LAM structure is attributed to a highly strengthened IMDS flattening, as the columnar LC phase could act on both ends of the PS block of the ABA DJBCP.

We note that the oriented scattering pattern in Figure 5a for the as-cast film of the ABA DJBCP indicates that the film comprises hierarchically ordered domains of a domain size larger than the SAXS beam size used (diameter 250 μm), hence the single-domain scattering pattern. The HEX_{col}-*within*-LAM structure with edge-on LAM orientation should be a solvent-trapped structure during solution casting. The corresponding volume fraction of the dendron-jacket domains $\phi_{DB} = 0.32$ can be extracted from the TEM image and SAXS scattering results (Figure 5), based on the lamellar spacing 23.3 nm and an average $P4VP(TOB)_{0.7}$ layer thickness of 7.5 nm deduced. The deduced ϕ_{DB} value for the columnar LC phase is only ca. half of that ($\phi_{0\text{-}DB} = 0.62$) calculated based on an ideal mixing without LC packing of the ABA DJBCP. Presumably, during annealing with weaken hydrogen bonding, the diminished LC packing strength could lead $\phi_{DB} \approx \phi_{0\text{-}DB} = 0.62$, resulting a minority of PS phase ($\phi_{PS} \approx 0.38$) for formation of hexagonally packed cylinders HEX_{CYL}. In a subsequent stretching-annealing process for enhanced hydrogen bonding and π–π stacking within the $P4VP(TOB)_{0.7}$ complex,[23] the columnar LC phase could form and drive the DJBCP to a thermally stable hierarchical structure of HEX_{col}-*within*-HEX_{CYL}.

Shown in Figure 6a and Figure S6 are the SAXS patterns taken respectively with the beam incidences parallel and perpendicular to the cylinder axis of the ABA DJBCP film after stretching-annealing, revealing a hierarchically ordered HEX_{col}-*within*-HEX_{CYL} structure. These single-crystal-like reflections indicate highly uniaxially aligned HEX_{CYL} domains, with domain sizes at least as large as the SAXS beam size used (diameter 250 μm). In Figure 6a, the highly ordered, 6-fold symmetric reflections in the small-q region are indexed with a HEX_{CYL} structure; the corresponding lattice parameter $a = 28.5$ nm is ca. 6 nm smaller than that of PS_{230}-*b*-$P4VP_{90}(TOB)_{0.7}$, although both cases have similar volume fractions and total molecular weights. In the large-q region, the sharp arc-like reflections with peak position ratios $1:\sqrt{3}:2$ correspond well to the (10), (11), and (20) reflections of an HEX_{col} LC phase, with a lattice parameter $a_c = 4.7$ nm. Reflections of each set of

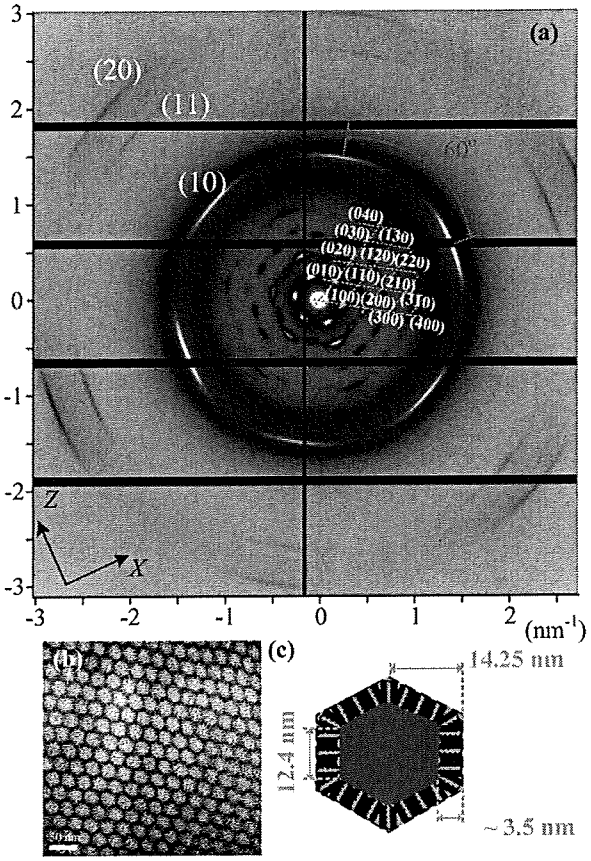

Figure 6. (a) 2D SAXS pattern with X-rays incident along the axial direction of PS cylinders (Y-direction) of a stretching-annealed film of $P4VP_{43}(TOB)_{0.7}$-*b*-PS_{260}-*b*-$P4VP_{43}(TOB)_{0.7}$. (b) Corresponding TEM image showing a honeycomb structure with hexagonal PS cells (bright domains). (c) A cartoon for the cross section of a hexagon cell comprising a hexagonal PS cylinder enclosed by a shell of $P4VP(TOB)_{0.7}$ columns.

HEX_{col} are well aligned along the respective azimuthal directions. An included angle 60° between any two adjacent sets of the six sets of HEX_{col} reflections implies perfect hexagonal PS cylinders with ideally flat IMDS, in contrast to the previous OBL structure (with slightly distorted hexagons) of the AB DJBCP (cf. Figure 1a).

A TEM micrograph in Figure 6b provides coherent evidence for the honeycomb-like structure, comprising hexagonal PS cylinders shelled with the $P4VP(TOB)_{0.7}$ LC columns. Note that the polygon edges of the hexagonal PS domains in the TEM image are not as sharp as the elongation-enhanced polygon edges of the distorted hexagons of the AB DJBCP of PS_{230}-*b*-$P4VP_{90}(TOB)_{0.7}$, due to the significantly smaller polygon edges. Nevertheless, the hexagon features can be identified reasonably well, compared to the circular PS domains shown in Figure 3b. We emphasize that polygon edges of the PS domains of a small size can be best illustrated with the perfect alignments of (10), (11), and (20) reflections of the HEX_{col} LC phase along the polygon edges as shown in Figure 6a. TEM image for short polygon edges of PS domains, however, could be easily deteriorated during TEM sample preparation with sectioning or imperfect iodine staining.

dx.doi.org/10.1021/ma501105p | *Macromolecules* 2014, 47, 6047–6054

As illustrated in Figure 6c, the side length of the PS hexagons, l = 12.4 nm, is deduced using the relation $l = (4/3)^{0.5}[(a/2) - t]$; the hexagon shell width $t \approx 3.5$ nm of the HEX_{col} LC domains is estimated from the TEM image in Figure 6b. As the diameter of each P4VP(TOB)$_{0.7}$ column is ca. 4 nm (observed in our previous work),[22] each side of the hexagon can hence accommodate roughly three LC columns of P4VP(TOB). Further deduction based on the TEM image and SAXS-revealed lattice parameters reveals a much larger volume fraction $\phi_{PS} = 0.57$ for the hexagonal PS cylinders, compared to $\phi_{0\text{-}PS} = 0.38$ calculated from the ABA DJBCP without LC packing. Such consequence suggests that chain conformation of the PS domains may be extended (about 1.22-fold as estimated from the squared root of $\phi_{PS}/\phi_{0\text{-}PS}$, assuming a constant of cylinder length) by the dendronized blocks of P4VP(TOB)$_{0.7}$ during formation of the columnar LC phase with flat IMDS. Correspondingly, $\phi_{DB} = 0.43$ for the P4VP(TOB)$_{0.7}$ blocks with the columnar LC phase is much smaller than $\phi_{0\text{-}DB} = 0.62$ when the columnar LC packing dissipates.[22] This result suggests a shrinkage of 31% in the dendronized block length to 3.5 nm during formation of the columnar LC phase. Jacked by TOB, the P4VP chains in the dendronized blocks are highly coiled and compressed (by 31%) in the columnar LC phase, as also detailed in our previous report.[23]

For comparison, the volume fraction of the hexagonal PS cylinders in the AB DJBCP case of PS$_{230}$-*b*-P4VP$_{90}$(TOB)$_{0.7}$ was also found to swell comparably from $\phi_{0\text{-}PS} = 0.33$ to $\phi_{PS} = 0.59$ (hence a PS chain stretching of 1.3-fold), when the dendronized blocks form a columnar LC phase. The PS chain extension for flat IMDS observed in both the AB and ABA DJBCP agrees with a theoretical prediction by Gido et al.[3] They suggested that IMDS of block copolymers might be modulated for Wigner–Seitz cells via deformation of chain conformation of the matrix blocks in cylinder-forming ABC triblock copolymers, provided that the volume fraction of the enclosed cylinder domains is close or above 0.6.

Interplay between Global Microphase Separation and Local LC Ordering. By modulating the LC packing strength of the dendronized block P4VP(TOB)$_{0.7}$ and, hence, the interplay between the global microphase separation of the DJBCP and the local LC ordering of P4VP(TOB)$_{0.7}$, we have demonstrated rich hierarchically ordered morphologies of AB and ABA DJBCP, such as an unconventional honeycomb structure with hexagonal cylinders or ultra-asymmetric lamellae. The 2D ordered HEX_{col} LC phase of presumably high curvature energy can compensate for the increase in interfacial energy with flat IMDS and direct self-assembly of the DJBCP to behave like rod–coil block copolymers. The dendronized blocks P4VP(TOB)$_{0.7}$ with a weaker smectic phase, however, cannot override the microphase separation of the copolymer dominated by the volume fractions of the PS and P4VP(TOB)$_{0.7}$ blocks.[29] In tuning the hierarchically ordered structures of the DJBCP, both volume fraction and LC packing strength of the dendronized blocks need to be considered. This conclusion is consistent with a supramolecular synergistic effect proposed previoulsy,[30,31] suggesting that DJBCP with a critically enhanced volume of the dendronized block can form long-range ordered microdomains. In our study, single-crystal-like structures of submillimeter domain sizes are observed with the two demonstrated cases PS$_{230}$-*b*-P4VP$_{90}$(TOB)$_{0.7}$ and P4VP$_{43}$(TOB)$_{0.7}$-*b*-PS$_{260}$-*b*-P4VP$_{43}$(TOB)$_{0.7}$.

We emphasize that formation of high strength columnar LC phases in the DJBCP relies critically on the TOB grafting density of $x = 0.7$ for a strong but balanced self-packing strength of the dendronized block. As shown in our previous report,[22] the dendronized blocks P4VP(TOB)$_x$ could only form smectic phases with the TOB grafting density $x < 0.5$, whereas a columnar LC phase could only form with $x \geq 0.5$. The TOB grafting ratio, however, saturates approximately at $x > 0.8$ due to steric effects of the fan-like shape of TOB molecules,[25] resulting in macrophase-separated crystalline domains of TOB (Figure S7).

CONCLUSIONS

We have demonstrated that a 2D-ordered HEX_{col} LC phase of the dendronized block P4VP(TOB)$_{0.7}$ can substantially flatten the IMDS morphology and direct the self-assembly of the AB and especially the ABA DJBCP studied. Hexagonal PS cylinders are consequently formed in the global HEX_{CYL} or OBL_{CYL} phase, leading to highly oriented and ordered hierarchical structures in a large length scale of submillimeter. As IMDS in a DJBCP needs to conform the shape with the global Wigner–Seitz cells of the microdomain lattices, our result may provide a promising approach in designing microdomains of various polygon shapes via tunable LC packing strength. Thereby, hierarchical structures of the DJBCP with greatly flattened IMDS and downsized microdomains could be expected as templates of highly oriented nanochannels or gratings with sharp edges.

ASSOCIATED CONTENT

Supporting Information

SAXS and WAXS results of PS-*b*-P4VP(TOB)$_{0.7}$. This material is available free of charge via the Internet at http://pubs.acs.org.

AUTHOR INFORMATION

Corresponding Authors

*Tel 8863-5780281 ext 7125; Fax 8863-5783813; e-mail weitsung@nsrrc.org.tw (W.-T.C.).

*Tel 8863-5780281 ext 7108; Fax 8863-5783813; e-mail usjeng@nsrrc.org.tw (U.-S.J.).

Notes

The authors declare no competing financial interest.

ACKNOWLEDGMENTS

Financial support from the National Science Council (Grants MOST 103-2221-E-213-002 and MOST 102-2112-M-213-005-MY3) is gratefully acknowledged.

REFERENCES

(1) Jeong, J. W.; Park, W. I.; Kim, M.-J.; Ross, C. A.; Jung, Y. S. *Nano Lett.* **2011**, *11*, 4095.

(2) Thomas, E. L.; Lescanec, R. L. *Philos. Trans. R. Soc. London, Ser. A* **1994**, *348*, 149.

(3) Gido, S. P.; Schwark, D. W.; Thomas, E. L.; Goncalves, M. *Macromolecules* **1993**, *26*, 2636.

(4) Lescanec, R. L.; Fetters, L. J.; Thomas, E. L. *Macromolecules* **1998**, *31*, 1680.

(5) Takahashi, K.; Hasegawa, H.; Hashimoto, T.; Bellas, V.; Iatrou, H.; Hadjichristidis, N. *Macromolecules* **2002**, *35*, 4859.

(6) Sioula, S.; Hadjichristidis, N.; Thomas, E. L. *Macromolecules* **1998**, *31*, 5272.

(7) Asai, Y.; Yamada, K.; Yamada, M.; Takano, A.; Matsushita, Y. *ACS Macro Lett.* **2014**, *3*, 166.

(8) Lee, M.; Cho, B. K.; Kim, H.; Yoon, J. Y.; Zin, W. C. *J. Am. Chem. Soc.* **1998**, *120*, 9168.
(9) Tung, S. H.; Xu, T. *Macromolecules* **2009**, *42*, 5761.
(10) Mezzenga, R.; Ruokolainen, J.; Fredrickson, G. H.; Kramer, E. J.; Moses, D.; Heeger, A. J.; Ikkala, O. *Science* **2003**, *299*, 1872.
(11) Mezzenga, R.; Ruokolainen, J.; Hexemer, A. *Langmuir* **2003**, *19*, 8144.
(12) Ruokolainen, J.; Mäkinen, R.; Torkkei, M.; Mäkelä, T.; Serimaa, R.; ten Brinke, G.; Ikkala, O. *Science* **1998**, *280*, 557.
(13) Ikkala, O.; ten Brinke, G. *Science* **2002**, *295*, 2407.
(14) Valkama, S.; Kosonen, H.; Ruokolainen, J.; Haatainen, T.; Torkkeli, M.; Serimaa, R.; ten Brinkn, G.; Ikkala, O. *Nat. Mater.* **2004**, *3*, 872.
(15) Polushkin, E.; van Ekenstein, G. A.; Dolbnya, I.; Bras, W.; Ikkala, O.; ten Brinke, G. *Macromolecules* **2003**, *36*, 1421.
(16) van Ekenstein, G. A.; Polushkin, E.; Nijland, H.; Ikkala, O.; ten Brinke, G. *Macromolecules* **2003**, *36*, 3684.
(17) Canilho, N.; Kasel mi, E.; Schlu1ter, A. D.; Ruokolainen, J.; Mezzenga, R. *Macromolecules* **2007**, *40*, 7609.
(18) Lee, W. B.; Richard Elliott, R.; Mezzenga, R.; Fredrickson, G. H. *Macromolecules* **2009**, *42*, 849.
(19) Merlet-Lacroix, N.; Rao, J.; Zhang, A.; Schlu1ter, A. D.; Bolisetty, S.; Ruokolainen, J.; Mezzenga, R. *Macromolecules* **2010**, *43*, 4752.
(20) Mezzenga, R.; Ruokolainen, J.; Canilho, N.; Kasemi, E.; Schluter, D. A.; Lee, W. B.; Fredricksone, G. H. *Soft Matter* **2009**, *5*, 92.
(21) Li, C.; Schlüter, A. D.; Zhang, A.; Mezzenga, R. *Adv. Mater.* **2008**, *20*, 4530.
(22) Chuang, W. T.; Sheu, H. S.; Jeng, U. S.; Wu, H. H.; Hong, P. D.; Lee, J. J. *Chem. Mater.* **2009**, *21*, 975.
(23) Chuang, W. T.; Huang, Y. S.; Su, C. J.; Jeng, U. S.; Sheu, H. S. *Soft Matter* **2012**, *8*, 11163.
(24) Jeng, U. S.; Su, C. H.; Liao, K. F.; Chuang, W. T.; Lai, Y. H.; Chang, J. W.; Chen, Y. I.; Huang, Y. S.; Lee, M. T.; et al. *J. Appl. Crystallogr.* **2010**, *43*, 110.
(25) Wang, S. J.; Xu, Y. S.; Yang, S.; Chen, E. Q. *Macromolecules* **2012**, *45*, 8760.
(26) Klok, H. A.; Langenwalter, J. F.; Lecommandoux, S. *Macromolecules* **2000**, *33*, 7819.
(27) Horsch, M. A.; Zhang, Z.; Glotzer, S. C. *J. Chem. Phys.* **2006**, *125*, 184903.
(28) Horsch, M. A.; Zhang, Z.; Glotzer, S. C. *Soft Matter* **2010**, *6*, 945.
(29) Hamley, I. W. *The Physics of Block Copolymers*; Oxford University Press: Oxford, UK, 1998.
(30) Muthukumar, M.; Ober, C. K.; Thomas, E. L. *Science* **1997**, *277*, 1225.
(31) Yu, H.; Kobayashi, T.; Yang, H. *Adv. Mater.* **2011**, *23*, 3337.